

AD-A198 093

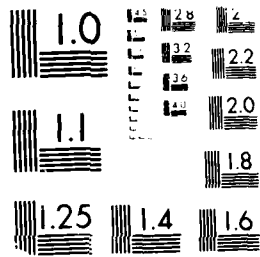
EVOLUTION OF GRAIN STRUCTURE IN NICKEL OXIDE SCALES(U)  
ATOMIC ENERGY RESEARCH ESTABLISHMENT HARWELL (ENGLAND)  
H U ATKINSON NOV 86 AERE-R-12372

1/1

UNCLASSIFIED

F/G 11/6.1 ML

END  
28



MICROCOPY RESOLUTION TEST CHART  
1010A

AERE R 12372

APPROVED FOR PUBLICATION

AERE R 12372

THIS DOCUMENT IS INTENDED FOR PUBLICATION IN THE OPEN LITERATURE. Until it is published, it may not be circulated, or referred to outside the organisation to which copies have been sent.

①

DTIC FILE COPY

AD-A190 093

United Kingdom Atomic Energy Authority

**HARWELL**

DTIC  
ELECTE  
S JAN 11 1988 D  
D

# Evolution of grain structure in nickel oxide scales

DISTRIBUTION STATEMENT A  
Approved for public release  
Distribution Unlimited

H V Atkinson

COPYRIGHT AND REPRODUCTION  
Enquiries about copyright and reproduction should be addressed to the Publications Office, AERE Harwell, Oxfordshire, England OX11 0RA.

Materials Development Division  
Harwell Laboratory, Oxfordshire OX11 0RA

November 1986

APPROVED FOR PUBLICATION

C14

87 12 00 000



## CONTENTS

	<u>Page No.</u>
1. INTRODUCTION	1
2. EXPERIMENTAL METHOD	3
2.1 Coupon Preparation and Oxidation	3
2.2 Transverse and Parallel TEM Specimen Preparation	4
2.3 TEM Specimen Examination and Tracing of Grain Boundary Networks	5
2.4 SEM of Fracture Sections	5
2.5 Measurement of Texture Coefficients	5
2.6 Image Analysis for Quantitative Grain Structure Information	6
3. RESULTS	7
3.1 Prediction of the Rate Controlling Grain Size, $G_R$	7
3.2 SEM Surface Morphology Observations	8
3.3 Parallel TEM Observations	8
3.4 Texture Coefficients	9
3.5 Grain Boundary Networks from Transverse TEM and SEM Observations	9
3.6 STEM Analysis for Impurities	9
3.7 Image Analysis	10
4. DISCUSSION	12
4.1 Oxide Islands	12
4.2 Surface Morphology Observations	13
4.3 Porosity	15
4.4 Parallel TEM Observations	16
4.5 Image Analysis and Texture Results	17
4.6 Discrepancy between $G_R$ and max. $\bar{x}_c$	22
4.7 Activation Energy for Grain Growth	25
5. SUMMARY, CONCLUSIONS AND SUGGESTIONS FOR FURTHER WORK	25
ACKNOWLEDGEMENTS	28
REFERENCES	29

## TABLES

1. XRD texture coefficients for NiO scales.	31
---	----

### ILLUSTRATIONS

- Fig. 1 Diagram illustrating parallel and transverse TEM sections.
- Fig. 2 Schematic diagram illustrating the rate controlling grain size,  $G_R$ , in a typical NiO scale grain structure.
- Fig. 3 Schematic diagram illustrating the image analysis parameters.
- Fig. 4 Plots of predicted rate controlling grain size,  $G_R$ , versus time  $t$ . Lower graph oxidations at 800°C and 1000°C, upper graph oxidations at 700°C.  $G_R$  calculated from weight gain data.
- Fig. 5 SEM micrographs at 0° tilt of oxide surface morphologies after  $\frac{1}{2}$  hour oxidation.  
(a) Specimen 46, 1000°C,  $\frac{1}{2}$  hour.  
(b) Specimen 65, 800°C,  $\frac{1}{2}$  hour.
- Fig. 6 SEM micrographs at 0° tilt of oxide surface morphologies after 4 hours oxidation.  
(a) Specimen 62, 1000°C, 4 hours.  
(b) Specimen 59, 800°C, 4 hours.
- Fig. 7 SEM micrographs at 0° tilt of oxide surface morphologies after 16 hours oxidation at 800°C and after 18 hours at 1000°C.  
(a) Specimen 48, 1000°C, 18 hours.  
(b) Specimen 74, 800°C, 16 hours.
- Fig. 8 Parallel TEM micrographs of stripped nickel oxide scales.  
(a) Scale grown at 1000°C for  $\frac{1}{2}$  hour (Specimen 46).  
(b) Scale grown at 800°C for  $\frac{1}{2}$  hour (Specimen 65).  
(c) Scale grown at 700°C for  $\frac{1}{2}$  hour (Specimen 53).
- Fig. 9 Parallel TEM of stripped nickel oxide scale grown at 800°C for 4 hours (Specimen 59).
- Fig. 10 Transverse TEM micrograph of scale grown on Ni at 700°C for 2 hours (Specimen 72) showing convolution of the outer surface of the oxide.
- Fig. 11 Transverse TEM micrograph of scale grown on Ni at 800°C for 21 hours (Specimen 58).
- Fig. 12 Transverse TEM micrograph of scale grown on Ni at 1000°C for 4 hours (Specimen 62).
- Fig. 13 SEM micrograph of transverse fracture section through scale formed on nickel at 1000°C for 18 hours in 1 atm. O<sub>2</sub> (Coupon 48).

ILLUSTRATIONS (Continued)

- Fig. 14 Grain boundary networks.  
(a) Specimen 70, area A, 700°C,  $\frac{1}{2}$  hour.  
(b) Specimen 73, area D, 700°C, 4 hours.  
(c) Specimen 54, area B, 700°C, 15 hours.  
(d) Specimen 65, area B, 800°C,  $\frac{1}{2}$  hour.  
(e) Specimen 59, area C, 800°C, 4 hours.  
(f) Specimen 58, area A, 800°C, 21 hours.  
(g) Specimen 46, area A, 1000°C,  $\frac{1}{2}$  hour.  
(h) Specimen 62, 1000°C, 4 hours (right hand image from SEM of fracture section).  
(i) Specimen 48, 1000°C, 10 hours, SEM of fracture section.
- Fig. 15 Plots of  $\bar{x}_c$  versus distance from the Ni/NiO interface. Points marked with S from SEM rather than TEM.  
(a) 700°C, 4 hours.  
(b) 800°C, 4 hours.  
(c) 1000°C, 4 hours.
- Fig. 16 Plot of  $\bar{x}_c$  versus time for layer adjacent to the Ni/NiO interface.
- Fig. 17 Plot of  $(\bar{y}_c/\bar{x}_c)$  versus distance from the Ni/NiO interface for scale grown at 700°C for 15 hours.
- Fig. 18 Plots of mean curvature/grain,  $\bar{k}$ , versus distance from the Ni/NiO interface.  
(a) 700°C, 4 hours.  
(b) 800°C, 21 hours.
- Fig. 19 Scale microstructure resulting from decrease in nucleation of new grains at outer surface as oxide thickens according to Tinker (1984). Outer columnar grains can grow laterally.

## 1. INTRODUCTION

The rate of oxidation of nickel, and of other transition metals of importance in gas-cooled nuclear reactor technology including chromium and iron, is controlled by outward diffusion of metal cations through the oxide scale<sup>(1)</sup>. For nickel, at temperatures in the region 500-1000°C, the grain boundary diffusion of cations dominates over that in the oxide lattice<sup>(2)</sup>. The grain structure of the scale is thus an important factor at these temperatures. The aim of this research was to extend understanding of the evolution of grain structure in nickel oxide scales. These scales can be used as a model for more complex oxide scales such as chromium oxide.

Control of the rate of oxidation by grain boundary diffusion of nickel cations through the oxide has been proved quantitatively for nickel<sup>(3)</sup> by measuring experimental oxidation rate constants,  $k_p$ , and comparing them with  $k_p$  values predicted using the expression:

$$k_p = 6.4 \left\{ D_L^* + \frac{2(D_{gb}^* \delta)}{G_R} \right\} \quad (1)$$

where  $D_L^*$  is the tracer lattice diffusion coefficient for nickel cations in NiO,  $D_{gb}^*$  the tracer grain boundary diffusion coefficient,  $\delta$  the grain boundary width and  $G_R$  the "rate controlling grain size".  $D_L^*$  and  $(D_{gb}^* \delta)$  have been measured independently<sup>(2)</sup> and values of the oxide grain size found by parallel Transmission Electron Microscopy (TEM) (Figure 1) of the scales at mid-thickness. The agreement between the experimental and predicted rates is good. In Figure 2 a schematic microstructure is shown.  $G_R$  is expected to be the largest average grain width for any plane parallel to the Ni/NiO interface. Parallel TEM only reveals the grain size in one plane though and transverse TEM (Figure 1) is required to examine the whole cross-section of the grain structure.

For other systems such as the oxidation of chromium and iron, although no quantitative proof of rate control by cation grain boundary diffusion has been obtained, there are strong parallels with nickel oxidation<sup>(1)</sup>.

Although the grain structure of oxide scales is an important factor in controlling the oxidation rate for temperatures less than  $T_m/2$  (where  $T_m$  is the melting point of the oxide) understanding of the microstructural evolution has only recently begun to develop, aided by transverse section TEM<sup>(4-6)</sup>. The transverse TEM studies reported in the literature have mainly been for NiO scales formed by oxidation of Ni at 1000°C.

The four main objectives of the experiments reported here are given below.

- (i) To obtain a (time, temperature) matrix of quantitative NiO scale grain structure information from transverse TEM and SEM observations, including temperatures lower than 1000°C.
- (ii) To correlate this information with parallel TEM and surface morphology Scanning Electron Microscopy (SEM) observations, and with X-ray Diffraction (XRD) texture coefficient measurements.
- (iii) Dividing the scale into layers parallel to the Ni/NiO interface and finding the average grain width,  $\bar{x}_c$ , for each layer (Fig. 3), to check how closely the maximum  $\bar{x}_c$  agrees with the rate controlling grain size,  $G_p$ , predicted from the oxidation rate via equation (1).
- (iv) To examine trends in  $\bar{x}_c$  with time, temperature and distance from the interface and whether correlations exist between  $\bar{x}_c$  and the mean columnar tendency ( $\bar{y}_c/\bar{x}_c$ ) (where  $y_c$  is the grain length perpendicular to the Ni/NiO interface) (Fig. 3). For columnar grains  $(\bar{y}_c/\bar{x}_c) > 1$ .
- (v) To find whether the mean curvature per grain,  $\bar{k}$  (see Fig. 3) correlates with tendency for grain growth as it is thought to do in bulk grain growth theory<sup>(7,8)</sup>.

The purpose of objective (iii) was to extend the work of Atkinson et al.<sup>(3)</sup> where the grain sizes substituted into the analysis were those from parallel TEM at mid-thickness with little knowledge as to the variation in grain size with depth in the scale. The transverse TEM observations reported here allow more detailed assessment of the degree of agreement between the predicted grain size and the observed grain sizes in the scale. The maximum  $\bar{x}_c$  is expected to be the rate controlling grain size,  $G_R$ .

Grains in scales tend to become columnar, i.e. their length perpendicular to the Ni/NiO interface is greater than their width. The purpose of objective (iv) was to find under what conditions the columnar tendency develops and whether  $\bar{x}_c$  tends to a constant value when  $(\bar{y}_c/\bar{x}_c) > 1$ , so that only  $\bar{y}_c$  increases as scale growth continues. In this case, the columnar grain boundaries do not move laterally. (Lateral movement is shown schematically in Figure 2).

Objective (v) is connected with the discussion about "structural gradient" in the literature on bulk grain growth theory<sup>(7,8)</sup>. The structural gradient is thought to represent the tendency of a structure to undergo grain growth. Here only the simple parameter of mean curvature/grain (as defined in Fig.3) will be considered. This is one step towards the more complex definitions of structural gradient in the literature. Small grains with large curvature (the curvature  $k$  is inversely related to  $R$  where  $R$  is the radius of curvature) will grow or shrink fast. Large grains with more gently curved boundaries will grow more slowly. The question for investigation is whether the mean curvature/grain is a useful parameter for oxide scales or whether other factors intervene.

## 2. EXPERIMENTAL METHOD

### 2.1 Coupon Preparation and Oxidation

"Puratronic" polycrystalline nickel coupons (supplied by

Johnson Matthey Chemicals Ltd., with < 25 ppm metallic impurities\*) were polished and annealed then light polished to a 1  $\mu$ m diamond finish. The 1 cm<sup>2</sup> coupons were oxidised in a specially built rig<sup>(9)</sup> at 700°C, 800°C and 1000°C for times between  $\frac{1}{2}$  hour and 20 hours in research grade (99.98% pure) dry oxygen at 1 atmosphere pressure. The coupons were accurately weighed before and after oxidation to find the weight gain during oxidation. Details of coupon preparation prior to oxidation, and of preparation of specimens for microstructural examination, are given in reference 10. After oxidation, oxide surface morphology observations were made with SEM.

## 2.2 Transverse and Parallel TEM Specimen Preparation

To prepare transverse TEM specimens a strip 2.8 mm wide was cut from the oxidised coupon and coated with nickel by Sputter Ion Plating (SIP). This holds the oxide in place during subsequent specimen preparation and protects the outer surface of the oxide from excessive milling during ion beam thinning. Slices 0.6 mm wide were cut out of the strips and ground and polished to ~ 50  $\mu$ m thickness with a Gatan hand grinder. The slices were further reduced in thickness by dimpling and spot welded at either end onto 3 mm diameter stainless steel washers for ease of specimen handling. Each slice was ion beam thinned until regions of the oxide were electron transparent.

Parallel TEM specimens were obtained by dissolving away the nickel substrate from the remaining part of the oxidised coupon, after removal of the strip for transverse TEM specimen preparation, with a saturated solution of iodine in absolute alcohol. The stripped scale was then ion beam thinned to electron transparency, from one side only, so as to reveal either the outer or the inner part of the scale.

---

\* A typical coupon was analysed by Inductively Coupled Plasma Emission Spectroscopy (ICPES) after surface preparation and prior to oxidation, and found to contain (ppm by weight): < 0.5 Ag, < 2 Al, < 0.2 Ba, < 2 Ca, < 0.5 Cr, < 2 Cu, 4 Fe, < 5 Mg, < 0.1 Mn, < 3 Si, < 0.1 Y, < 1 Zr.

### 2.3 TEM Specimen Examination and Tracing of Grain Boundary Networks

The parallel and transverse TEM specimens were examined at 300 kV in a Philips EM430 Transmission Electron Microscope. For quantitative grain size information, transverse TEM micrographs were obtained with both tilts at 0° and grain structures traced. Structures were sometimes difficult to discern and judgement had to be used to obtain networks, e.g. joining "hanging" grain corners where the boundary between the corners was not in the correct orientation to give contrast. The enhanced penetrating power of the 300 kV instrument is an advantage over conventional 100 kV TEMs but brings further errors in deciding where to place boundaries when grain boundary fringes (e.g. Figure 11) and grain overlaps are visible. The NiO/SiP Ni interface was identified with a windowless Energy Dispersive X-ray Analyser (which can detect oxygen X-rays) in a VG HB501 Scanning Transmission Electron Microscope (STEM). The presence of impurities in the scales was also checked for in the STEM.

### 2.4 SEM of Fracture Sections

For scales thicker than  $\sim 10 \mu\text{m}$  (i.e. grown for times of 4 hours or longer at 1000°C) it was difficult to obtain thinned sections showing the structure across the whole scale. In addition, the grains were sufficiently large for only a few to be visible in each electron transparent area, with consequently poor statistics. Therefore, for these thick scales, oxide stripped from the metal by metal dissolution was fractured and examined edge-on in the SEM to obtain at least some quantitative information on grain sizes.

### 2.5 Measurement of Texture Coefficients

Texture coefficients were obtained by comparing heights of low-index peaks in spectra, with random values for NiO in JCPDS (Joint Council Powder Diffraction Standard). Ideally the reference should be a sample of large strain-free NiO crystallites examined in the Harwell diffractometer, but such material was not available. In general, if the texture coefficient is greater than 1 for a particular set of planes it indicates that there is a preponderance of NiO grains in the scale.

oriented such that those planes are parallel to the surface. However, the lack of an ideal reference standard means that the absolute values of the texture coefficients should not be considered. Interpretation must be based on the relative magnitudes.

The texture coefficient for a given set of planes ( $h'k'l'$ ) is defined as:

$$T_{h'k'l'} = \frac{I_{h'k'l'} / I_{h'k'l'}^0}{\frac{1}{z} \sum_0 (I_{hkl} / I_{hkl}^0)} \quad (2)$$

where  $I_{hkl}$  and  $I_{hkl}^0$  are respectively the measured intensity, and the intensity in the case of a standard randomly oriented specimen, for the reflection ( $hkl$ ), and  $z$  reflections are considered.

#### 2.6 Image Analysis for Quantitative Grain Structure Information

For the traced grain boundary networks, each traced grain was analysed quantitatively in a Kontron IBAS Interactive Image Analysis System for:-

- i)  $x_c$ , the mean grain width parallel to the Ni/NiO interface
- ii)  $y_c$ , the mean grain length perpendicular to the Ni/NiO interface
- iii)  $h$ , the distance of the centre of gravity of the grain from the Ni/NiO interface.

These parameters are shown in Fig. 3.

In addition, two further parameters,  $k$ , the mean boundary curvature and  $n$ , the number of sides, were analysed for by hand.  $k$  was found by measuring each facet of a grain against a radius of curvature template (assuming the boundaries to be circular) and then finding the average.

i.e. 
$$k = \frac{1}{n} \sum_{i=1}^{i=n} \frac{1}{R_i} \quad (3)$$

where  $R_i$  is the radius of the  $i$ th facet. Further details of this method of finding radius of curvature are given elsewhere<sup>(11)</sup>. The errors are large (mainly from tracing the network in the first place), but general trends can be examined.

Each scale was divided into layers parallel to the Ni/NiO interface and the means  $\bar{x}_c$ ,  $(\bar{y}_c/\bar{x}_c)$ ,  $\bar{k}$  and  $\bar{n}$  found for the grains in each layer (see Figure 3). A grain is defined as lying within a layer if its centre of gravity lies within the layer.

### 3. RESULTS

#### 3.1 Prediction of the Rate Controlling Grain Size, $G_R$

The oxide thickness  $X$  is calculated from the weight gain during oxidation  $w$ , assuming the oxide is uniform in thickness, pore free and grows at the same rate on the edges as on the plane surfaces, using

$$X \text{ (in } \mu\text{m)} = \frac{3.5 w \text{ (in mg)}}{(A_c + 2t_c) \text{ (in cm}^2\text{)}} \quad (4)$$

where  $A_c$  is the area of a single side of the coupon and  $t_c$  its thickness prior to oxidation. In deriving the formula, it is assumed that the coupon has one centimetre length sides.

The instantaneous parabolic oxidation rate is given by

$$k_p = \frac{d}{dt} (X^2) = \frac{2X^2}{t} \frac{d(\log X)}{d(\log t)} \quad (5)$$

where  $t$  is the time. Hence,  $k_p$  can be calculated knowing  $X$ ,  $t$  and the gradient in the plot of  $\log X$  versus  $\log t$ .

$k_p$  can then be substituted into equation (1) and knowing  $D_L^*$  and  $(D_{gb}^* \delta)$  from experiment<sup>(2)</sup>,  $G_R$  can be found. The derivation of

equation (1) assumes a uniform square array of grains with dimension  $G_R$  parallel to the Ni/NiO interface.

The  $G_R$  values are plotted against oxidation time in Figure 4. The errors shown are those expected from measurement of  $w$  and  $A_c$ , from the assumptions in calculating  $X$ , and from finding the gradient  $d(\log X)/d(\log t)$ . The error due to assuming the scale is a uniform square array of grains will be discussed later and is not shown. A, B and C refer to slightly different coupon preparations prior to oxidation and are discussed elsewhere<sup>(10)</sup>. Points marked with numbers are those for specimens whose scales were later examined by transverse TEM or SEM of fracture sections.

### 3.2 SEM Surface Morphology Observations

Representative micrographs are shown in Figures 5, 6 and 7 for 800°C and 1000°C scales. The 700°C structures are similar to those for 800°C, but finer in scale. At both temperatures, the surfaces exhibit cavities which tend to close up as time increases (compare Figure 5(b) with Figure 7(b)).

At 1000°C, after  $\frac{1}{2}$  hour, ridges of material are present on the surface with some surface cavities (Figure 5(a)). The ridges are extensively buckled. By 4 hours, the structure has become coarser (Figure 6(a)) with ridges still present, but developing trenches, e.g. at A. There are few cavities present and fine surface detail is beginning to appear, e.g. at B. Between 4 hours and 18 hours, the ridges disappear (Figure 7(a)). The boundary trenches become faceted (e.g. at C) and surface features within the grains enhanced (e.g. at D). These surface features may be associated with the intersection of dislocations with the surface.

### 3.3 Parallel TEM Observations

Typical micrographs are shown in Figure 8 and 9. At 700°C and 800°C the trends are similar. Initially the oxide consists of a fairly confused matrix with a few large grains visible in diffraction contrast (see Figures 8(b) and 8(c)). With increasing time, the parallel sections

begin to exhibit areas of well developed grain structure (see Figure 9), but the boundaries are still curved to a certain extent, indicating that a driving force for grain growth still exists.

At 1000°C, the grain structure is fairly regular even after only  $\frac{1}{2}$  hour (see Figure 8(a)). After 8 hours the boundaries retain some curvature.

#### 3.4 Texture Coefficients

The texture coefficient results are given in Table 1. At 1000°C, {220} dominates (except at 4 hours where {111} is the major component). At 800°C and 700°C, {200} is the predominant grain orientation.

#### 3.5 Grain Boundary Networks from Transverse TEM and SEM Observations

Typical transverse TEM micrographs are shown in Figures 10, 11 and 12 and a typical SEM fractograph in Figure 13. Typical boundary networks are shown in Figure 14. The grain structure is not clear in Figure 10 (for oxide grown at 700°C for 2 hours) but the figure is shown to illustrate the marked bulging in the NiO/SiP Ni interface for 700°C specimens. For early times at 700°C ( $\frac{1}{2}$  hour) and at 800°C ( $\frac{1}{2}$  hour) there were regions of the nickel substrate surface where no oxide could be detected by STEM between the oxide islands (see networks in Figure 14(a)). Faceted porosity is evident in transverse sections through the NiO (see Figure 11).

For longer times at 700°C and 800°C, the structure became more clearly discernible. At 1000°C the grains were well-developed from as early as  $\frac{1}{2}$  hour. Scales grown at 700°C and 800°C tended to consist, after about an hour, of several layers of grains (e.g. Figure 11). Only a few layers were present in scales grown at 1000°C (Figure 12).

#### 3.6 STEM Analysis for Impurities

Several transverse TEM specimens were examined by STEM. Mn, Fe and Cr were detected at grain boundaries, Fe and Cr in the matrix. The levels were estimated as anything up to ~ 10%. Given the initial purity of the nickel coupons and the measures taken during specimen preparation and oxidation to avoid contamination, Fe and Cr at these high levels, particularly in the matrix, almost certainly originate from

sputtering of the stainless steel washer during thinning. Fe and Cr were also present as the only detectable impurities in the parallel TEM specimens. Mn was not detected in the parallel TEM specimens and the presence of Mn-based particles in the SIP Ni close to the oxide in transverse TEM sections suggests the Mn diffuses into the scale during the Sputter Ion Plating process. The plating nickel is commercial purity and contains Mn. Estimates of the diffusion coefficient for Mn in NiO grain boundaries at 400-500°C (the range in which the plating is carried out) suggest that penetration into the scale is feasible.

Hence, Mn can be discounted as a possible impurity influencing boundary migration during oxidation. However, Fe and Cr cannot be ruled out. It is not possible from the evidence to discern whether the Fe and Cr present in the grain boundaries and the matrix are purely due to sputtering from the washers, or whether there are small amounts in the oxide originating from the metal substrate (typically containing 4 ppm Fe by weight and < 0.5 ppm Cr from the ICPEs analysis cited earlier). 1 ppm of an impurity in the substrate could give rise to a few % at the oxide grain boundaries if it segregated totally to these sites during the oxidation process.

### 3.7 Image Analysis

The scales were divided into layers outwards from the Ni/NiO interface (1.0  $\mu\text{m}$  wide for 1000°C, 0.5  $\mu\text{m}$  wide for 800°C, 0.2  $\mu\text{m}$  wide for 700°C) and the means  $\bar{x}_c$ ,  $(\bar{y}_c/\bar{x}_c)$ ,  $\bar{k}$  and  $\bar{n}$  found for each layer (as illustrated in Figure 3). The layer width is a compromise between the requirement for a large number of grains to lie in a layer in order to obtain reasonable statistics when finding means and the requirement to be able to discern trends in grain size in the scale. It must be commented here that even with the layer widths chosen there are often only a few grains in each layer, particularly at 1000°C and towards the outer part of the scale. The errors are therefore large.  $\bar{x}_c$ ,  $(\bar{y}_c/\bar{x}_c)$ ,  $\bar{k}$  and  $\bar{n}$  were plotted against distance from the interface, (i.e. mid-point of the layer relative to the interface), and time, for the three temperatures. Dashed lines indicate the general trends. Significant results are listed with selected plots.

1.  $\bar{x}_c$  tends to rise sharply moving away from the interface then level off (800°C) or increase fairly steadily (1000°C) (see Figure 15) There is sometimes a drop in  $\bar{x}_c$  near the outer surface of the oxide (e.g. Figure 15(c)). For most specimens, transverse TEM information on the grain structures was obtained from more than one area of the coupon but no one area gave consistently higher grain sizes than another. However, two areas of oxide were examined for the (700°C, 4 hours) specimen, with quite different oxide thicknesses and  $\bar{x}_c$  results for each (see Figure 15(a)).
2.  $\bar{x}_c$  results from SEM fracture sections may be misleadingly low (for example see Figure 15(c) where the SEM results always lie below those from TEM).
3. Apart from in the layers adjacent to the interface, for times > 4 hours at 800°C and 1000°C,  $\bar{x}_c$  for a given layer is fairly constant with time (0.4-0.6  $\mu\text{m}$  for 800°C, 2.5-3.5  $\mu\text{m}$  for 1000°C).
4. At the interface, at 700°C,  $\bar{x}_c$  is approximately constant ( $\sim 0.1 \mu\text{m}$ ) with time and at 800°C and 1000°C rises gently (after an initial increase at 1000°C) over 20 hours (see Figure 16).
5. The maximum  $\bar{x}_c$  for a particular time and temperature is plotted onto Fig. 4 for comparison with the predicted rate controlling grain size  $G_R$ . The values lie consistently lower than those for  $G_R$ .
6. The columnar tendency,  $(\bar{y}_c/\bar{x}_c)$ , increases with increasing distance from the interface, increasing time and increasing temperature. At 700°C there is barely any columnar tendency at all (Figure 17) (i.e.  $\bar{y}_c/\bar{x}_c \sim 1$ )  $\bar{x}_c$  for a given layer and temperature is approximately constant for columnar grains.

7. Mean curvature per grain,  $\bar{k}$ , is high at the interface for short times and low temperatures (Figure 18(a)). It falls sharply to a fairly steady low level with distance from the interface. At longer times and higher temperatures the values at the interface tend to be approximately the same as those elsewhere in the scale (Figure 18(b)). Large grains have small curvature. (Note:  $k$  is inversely related to the radius of curvature.)
8. Grains close to the interface tend to have 3, 4 and 5 sides in the cross-section.  $\bar{n}$  is higher but fairly steady at greater distances from the interface.
9. The data was too scattered to find a grain growth law for grains in the scale whilst growth was occurring, prior to  $\bar{x}_c$  becoming approximately constant with time at a given distance from the interface. Hence, an activation energy of grain growth could not be obtained for comparison with theoretical predictions<sup>(14)</sup>.

#### 4. DISCUSSION

##### 4.1 Oxide Islands

Considering the surface morphology and transverse TEM observations together, at short times ( $\frac{1}{2}$  hour at 700°C and  $\frac{1}{2}$  hour at 800°C) the oxide is present in islands on the metal with areas between the islands where oxide is not detectable (although a thin layer,  $< 50 \text{ \AA}$  thick may be present). At longer times, the NiO/SiP Ni interface remains convoluted, corresponding with the surface 'cavities' seen in the SEM, although detectable oxide is present all over the metal. The NiO/Ni interface is cusped but there is no observable interfacial separation. This contrasts with  $\text{Cr}_2\text{O}_3$  formation on Cr where separation tends to occur in conjunction with the development of convoluted scales<sup>(15)</sup>. At longer times with the NiO scales, the cavities may still be up to 1  $\mu\text{m}$  deep, but shallow relative to the thickness of the oxide, particularly at 800°C.

The central question here is why the oxide grows in islands in the initial stages, even at 700°C and 800°C where oxidation rates are

relatively fast. Oxide islands have been observed by other investigators but only at lower temperatures and oxygen partial pressures<sup>(16-18)</sup>. It is possible that the island growth observed here may be associated with the start-up procedure. The specimen takes a finite time (a few minutes) to reach the oxidation temperature. Islands formed in the initial stages at relatively low temperatures may then grow preferentially if the energy required to deposit oxide on an existing island (either on existing grains or in new grains) is less than the energy required to deposit it on the bare metal (or very thin inter-island oxide). This might occur if the oxide grains in the islands are tending to have low energy {200} facets at the surface, as indicated by the texture measurements (see Table 1). {200} planes are expected to have relatively low surface energy<sup>(19)</sup>.

At longer times, the islands grow to impingement but to some extent the initial surface profile appears to be retained. This suggests that the grain structure in the first-formed islands is such that oxidation tends to be enhanced there, i.e. there is a smaller rate controlling grain size (or a smaller proportion of slow-diffusing boundaries - see later discussion of the discrepancy between  $G_R$  and  $\max \bar{x}_c$ ). At longer times and higher temperatures, this effect tends to be reduced and the surface profile is less indented.

The islands may be nucleated on surface heterogeneities such as dislocations or light polishing relief. It is not known what form they take in 3-D. 3-D information would give some pointers as to whether the nucleation is homogeneous or heterogeneous.

#### 4.2 Surface Morphology Observations

The separation between the ridges observed by SEM of the 1000°C specimen surfaces corresponds roughly with the grain width. The ridges may arise from:

- (a) Exaggerated oxide formation at oxide grain boundaries due to Ni cation vacancy migration predominantly along grain boundaries (seen as protuberances in transverse TEM by

Tinker<sup>(4)</sup>).

- (b) Stress generation leading to plastic deformation, squeezing the material up into ridges, or Coble creep (diffusional redistribution of material along the grain boundaries in response to stress).

Protuberances were not observed at the surface of the 1000°C scales in transverse TEM in this study. However, in most cases the NiO/SiP Ni interface was not retained for the 1000°C specimens. Where it was, the profile was difficult to discern as the material was relatively thick for TEM observations.

Dislocation activity is evident in the transverse TEM micrographs (e.g. Figure 12) providing evidence for stress generation, possibly due to the Rhines and Wolf new-oxide-within-oxide mechanism<sup>(20)</sup> or due to adhesion to a shrinking substrate. If the surface ridges are due to plastic deformation or creep, their separation suggests that the deformation is concentrating in the grain boundary regions. Features such as the flap of material at A in Figure 6(a) would appear to support ridges generated by stress more strongly than ridges generated by preferential oxidation. The relatively folded and buckled appearance of the ridges also supports this. Preferential oxidation ridges would tend to follow quite closely the smooth contours of grain boundaries intersecting the surface (as seen by parallel TEM for 1000°C - see Figure 8(a)).

The SEM surface morphology observations suggest that by 18 hours at 1000°C, either:

- (a) Stress generation has substantially decreased.
- or (b) Stress relief is occurring by some other mechanism than Coble creep or grain boundary deformation.
- or (c) Surface diffusion is dominating over cation grain boundary diffusion.

If stress generation occurs by either the Rhines and Wolf mechanism or adherence to the shrinking metal substrate, there appears to be no reason for a decrease with increasing time and if anything the stresses are expected to increase.

Stress relief without Coble creep might occur via Nabarro-Herring creep (diffusion in the bulk) or by dislocation climb. Nabarro-Herring creep is expected to be too sluggish at these temperatures though<sup>(21)</sup>. Dislocation climb also requires vacancy diffusion in the bulk, but not over such large distances as Nabarro-Herring creep. It is a possible stress relief mechanism in these circumstances but the formation of 'trenches' at the grain boundaries still cannot be explained. The possibility of grain boundary sliding which could contribute to surface relief must be mentioned. Kofstad has recently suggested that this might occur for scales<sup>(22)</sup>.

If surface diffusion is dominating over grain boundary cation diffusion, cations reaching the surface via grain boundaries are dispersed across the surface before oxide protuberances can form by reaction at the boundaries.

The confusing conclusion from this is that the surface ridges observed for earlier times at 1000°C can better be accounted for by plastic deformation or Coble creep in response to stress generation but the later time results (18 hours) suggest surface diffusion dominating over cation grain boundary diffusion. Perhaps in fact both explanations are correct in that both stress generation and exaggerated oxide formation are contributing to the development of ridges at short times. At longer times, the surface diffusion dominates and disperses material not only from cation grain boundary diffusion but also from grain boundary deformation and Coble creep.

#### 4.3 Porosity

Faceted porosity evident in transverse TEM micrographs (e.g. Figure 11) may arise from:

(a) Oxidation processes.

or (b) Ion beam thinning.

In oxidation, whilst cations are migrating outwards through the scale, cation vacancies are migrating inwards. Vacancies might also arise from diffusional flow during creep. These could agglomerate to form pores. In either case, the voids would be expected to be present mainly at grain boundaries and at higher density near the Ni/NiO interface than near the outer surface. Quantitative characterisation of the pore distributions was not carried out but qualitatively the voids did not appear to be concentrated at boundaries and near the interface, but rather to occur in "clumps".

Alternatively, the voids could arise from preferential sputtering during ion beam thinning. Ostyn and Carter have shown that preferential sputtering of oxygen can occur to such an extent that faceted nickel particles nucleate in NiO during ion thinning<sup>(23)</sup>. Nickel particles were not observed in the NiO in this study although they could have dropped out during specimen handling. In addition, ion thinning sometimes gives rise to complex surface relief and the voids could arise from this. Support for explanation (b) comes from the observation of some faceted porosity, of similar appearance to the voids in the NiO, in the SiPNi (Figure 10). There is counter-evidence though in Figure 13 where some relatively large size porosity (in comparison with that seen in the transverse TEM micrographs) appears to be visible on fracture surfaces on the SEM fractograph. This probably does arise from the oxidation process.

All that can be concluded here, without further research, is that the porosity observed in the transverse TEM micrographs probably arises from ion beam thinning whilst the more macroscopic pores seen in the SEM fractographs may originate in the oxidation process.

#### 4.4 Parallel TEM Observations

In metals, primary recrystallisation is relatively easy to identify because large strain-free (feature-free) grains are seen growing into a matrix with high dislocation density. Here, parallel TEM micrographs

for 700°C show a number of relatively large grains (much smaller than those generally observed in metals) in a confused matrix without a clear grain structure. The grain structure might not be apparent though if the specimens (which are very fragile) have not been thinned sufficiently and the grain size is extremely fine. Transverse TEM of short time scales grown at 700°C sometimes revealed clear small grain size structures but sometimes gave only a rather confusing image. Again this could be due to insufficient thinning or could be a real effect.

The evidence for primary recrystallisation in this research is equivocal. Sawhill and Hobbs have published one micrograph which appears to provide good evidence for primary recrystallisation in a furnace-cooled scale grown on mechanically polished Ni<sup>(6)</sup>

#### 4.5 Image Analysis and Texture Results

The image analysis results agree with the suggestion put forward by Tinker<sup>(4)</sup> that as the oxide thickens, the rate of nucleation of new grains at the oxide surface decreases (Fig. 19). This can probably best be understood as a kinetic effect. Whilst the oxide is being laid down relatively fast in the initial stages, there is insufficient time for new oxide units to orient so as to build on existing grains. Therefore, the nucleation rate is high. Ultimately, when the oxide is being laid down relatively slowly, no new grains are nucleated and the existing grains grow by extension of their lattice at the outer surface with fresh oxide. The grains are then columnar. As this condition is approached, the grains become increasingly columnar although new grains may occasionally be nucleated. Texture tends to develop either because certain grain orientations have faces with relatively low energies or because those faces grow faster. Thus columnar grains may increase in width with distance from the Ni/NiO interface even if there is no lateral columnar boundary migration. At the same time, certain grain orientations are occluded by the favoured grains.

Thus, at 800°C and 1000°C,  $\bar{x}_c$  increases initially with distance from the Ni/NiO interface and then becomes steady or only slowly increasing. The steady or slowly increasing width corresponds with columnar grains and a predominance of one grain orientation over others ( $\{200\}$  predominating at 1000°C,  $\{200\}$  at 800°C). At 800°C, the scales are thinner than at 1000°C. Therefore, the rate of nucleation is larger

and there are more grain layers in the scales (several for 800°C (Fig. 11), only a few for 1000°C (Fig. 12)). The existence of predominantly {200} grain orientations at 800°C may hence be due to preferential nucleation, whilst at 1000°C {220} may be favoured because these grains are tending to grow at the expense of other orientations.

The 700°C scales are only a few microns thick. The rate of nucleation is therefore expected to be large and consequently there is little or no columnar tendency (Fig. 17). Competition between the nucleation rate, scale thickening and boundary migration essentially determines the steady columnar grain width of 0.4-0.6  $\mu\text{m}$  at 800°C. A quantitative model to predict this width would be useful as this is the width which is expected to correspond to  $G_R$  (but see later discussion of the discrepancy between  $G_R$  and  $\bar{x}_c$ ). Similarly, at 1000°C the columnar grain width is slowly increasing in the region of 2.5-3.5  $\mu\text{m}$  and prediction of this rate of increase from grain competition would be valuable.

The significant differences in results for Areas A and D of the 700°C, 4 hours specimen may be associated with island growth. For instance, Area D might originally correspond with an inter-island area at early time. However, this specimen gave anomalous surface morphology results, possibly due to some unusual feature of the surface preparation procedure such as uneven light polishing, and therefore results from this specimen must be treated with circumspection.

The sharp fall in  $\bar{x}_c$  in the outermost layers of the scale for a few specimens is in some cases due to truncation of grains milled away during ion thinning. However, where the original NiO outer surface is preserved in the transverse TEM specimen it indicates that some newly nucleated grains are present.

At 800°C and 1000°C,  $\bar{x}_c$  increases initially with time for a given layer then tends to become steady (see Figs. 15(b) and 15(c)). This suggests some grain boundary migration is occurring in the initial stages. Once the grains are columnar though, the grain boundaries essentially become static. This could arise from:

- (a) Low grain boundary curvature.
- (b) Pinning by impurities (or pores).
- (c) Low concentration of the defects responsible for grain boundary migration in the outer part of the scale.
- (d) Pinning at the Ni/NiO interface or the NiO/O<sub>2</sub> interface.

There is evidence for low grain boundary curvature in the outer part of the scale (see Fig. 18). This is expected if the columnar grains intersect the outer surface and their boundaries are approximately perpendicular to the surface. However, the parallel TEM cross-sections reveal some quite curved boundaries even after 8 hours at 1000°C.

Pinning by impurities is difficult to deal with as the STEM composition measurements at grain boundaries in parallel sections showed Fe and Cr to be present. It is not clear whether these arise from contamination from the stainless steel support washer during ion beam thinning (see section 3.6). Examination of a parallel specimen supported on, for instance, a copper ring would have helped to identify whether impurities were present at the grain boundaries during oxidation. Copper is less likely to be a contaminant of the substrate nickel than Fe or Cr. The levels of impurities in the substrate are low (a few ppm or less). A few ppm in the substrate however, if segregated wholly to the boundaries in the oxide, could give significant levels. If impurities were present they would probably be concentrated in the inner part of the oxide and pin boundaries there. However, apart from at the interface itself at 700°C, boundary migration does appear to occur in the inner part of the scales, at least in the first few hours.

The pores observed have been discussed in Section 4.3. A fairly uniform distribution of pores would be required to inhibit boundary migration and such a uniform distribution was not found.

The anion vacancy concentration is expected to be lower in the outer part of the scale where the partial pressure of oxygen is

relatively high (e.g. see relationship derived by Dubois et al.<sup>(24)</sup>). Atomistic mechanisms of boundary migration in NiO are discussed in reference (14). If anion vacancy diffusion is responsible for boundary migration (assuming impurities are not controlling boundary migration) then a low anion vacancy concentration would give rise to low boundary migration rates. Conversely, rates in the inner part of the oxide would then be relatively high but in fact at the interface at 700°C the grain size is constant.

This latter result suggests there is pinning of grain boundaries by grooving at the Ni/NiO interface or by impurities concentrated close to the interface. The pinning decreases as the temperature increases but is probably still present to at least some extent even at 1000°C. The STEM measurements of impurity (Fe, Cr) concentrations did not indicate higher values than elsewhere close to the interface, although the impurity concentrations present during oxidation might be masked by the contamination from the washer (discussed in Section 3.6). Pinning by grooving would be associated with the cusps observed in the Ni/NiO interface where NiO grain boundaries intersect the interface and there is a tendency to equilibrate surface tension forces. The existence of these cusps tends to support this mechanism of pinning rather than impurities. This pinning effect differs from the specimen thickness effect, where grain growth ceases when metal grains span the whole thickness of the sheet because the metal boundaries then meet the surface at an angle less than a critical angle (deduced by Mullins<sup>(12)</sup> and the thermal grooves lead to pinning. Here pinning occurs for grains smaller than the thickness of the oxide but the nature of the oxidation process is such that boundaries intersecting the interfaces do tend to be perpendicular to it, allowing pinning when cusps are present. Pinning at the NiO/O<sub>2</sub> interface is unlikely except at 1000°C for long times, where the grain boundary trenches are equivalent to grooves.

Pinning at either interface by grooving might influence grains in layers not immediately adjacent to the interface through a 'knock-on' effect, i.e. if boundaries in one layer are constrained from moving, boundaries in the adjacent layer will be constrained through mechanical considerations<sup>(8)</sup> and so on. However, this cannot be a strong effect in the region of the Ni/NiO interface at 700°C (where pinning at that interface is most evident) as the grain size  $\bar{x}_c$  increases rapidly with

distance from the interface there.

Hence, of the four possible explanations for lack of lateral columnar boundary migration in the outer part of the oxide, low grain boundary curvature and low anion vacancy concentration might both contribute but pinning at interfaces is unlikely. Pinning by impurities cannot be ruled out. Further experiments would be required to distinguish between the possible explanations.

The effect of the vacancy concentration gradient and of Ni/NiO interface pinning could be examined by stripping the scale from the metal and annealing in an oxygen pressure of 1 atm. If grain growth in the inner part of the scale were then suppressed, low anion vacancy concentration is at least partly responsible for the lack of lateral grain boundary migration. However, it is likely that the relaxing of the pinning forces would dominate with rapid growth occurring. The pinning forces must be relatively strong for the grain size at the interface to be constant at 700°C and only slowly increasing at 800°C despite high convex boundary curvature  $\bar{k}$  (Fig. 18) and low  $\bar{n}$  both of which are expected to cause the grains in the region of the interface to shrink rapidly<sup>(8)</sup>. At 800°C there is some suggestion from the grain boundary networks that the small grains are shrinking into the interface as expected and larger grains from the next layer are then coming into contact with the interface.

As far as texture is concerned, {200} planes are expected to have relatively low surface energy<sup>(19)</sup>. As mentioned earlier, at 800°C  $\bar{x}_c$  is approximately steady with distance from the interface in the outer part of the scale. This suggests that the {200} texture is associated with preferential nucleation of new grains in the {200} orientation rather than with favoured growth causing occlusion of less favoured orientations and a gentle increase in  $\bar{v}_c$  with distance from the interface in the outer part of the scale. The latter explanation probably applies to the 1000°C scales where relatively fewer new grains are being nucleated but growth of {220} orientations is favoured.

The possibility that grain sizes from the SEM fractographs are systematically lower than the actual grain sizes, does not substantially affect the arguments above. However, it must be taken into account in consideration of the discrepancy between  $G_R$  and  $\max. \bar{x}_c$ .

Secondary recrystallisation may be occurring. Grains are observed with much greater  $n$  and  $x_c$  than surrounding grains (e.g. see Fig. 14) at 700°C and 800°C. In classic grain growth theory for metals, this would lead to the large grain growing at the expense of the smaller grains. However, the image analysis results, at least at 700°C, do not appear to support this; the small grains in the region of the interface are retained. The reason for this behaviour is not clear although it may be connected with the pinning at the Ni/NiO interface previously discussed. At 800°C, the small grains at the interface, do appear to be shrinking at the expense of larger grains further out. If this is occurring, it contrasts with conventional secondary recrystallisation for metals, which usually arises either from boundary pinning by a distribution of particles or from boundary energy anisotropy. Here boundary energy anisotropy may play a part but the large grains are essentially arising from the nature of the oxidation process itself, with the decrease in nucleation rate as the oxide thickens.

There appears to be no evidence for tertiary recrystallisation<sup>(e.g.25)</sup>. This is the exaggerated growth of a few non-randomly oriented grains at the expense of a matrix of finer grains (as in secondary recrystallisation) but driven by surface energy anisotropy, i.e. the surfaces of the exaggerated grains are oriented on low energy planes so that their growth leads to surface energy minimisation. This phenomenon might occur in oxide scales but grains with widths several times greater than the thickness of the oxide were not observed.

#### 4.6 Discrepancy between $G_R$ and $\max. \bar{x}_c$

The predicted rate controlling grain size  $G_p$ , is always larger than the maximum observed  $\bar{x}_c$  ( $\max. \bar{x}_c$ ) in a scale thickness (see Fig. 14). How is this discrepancy to be accounted for?

Firstly, it is useful to comment on the observed trends in  $G_R$  and  $\max. \bar{x}_C$ .  $G_R$  values increase fairly steadily for 1000°C, but after an initial rise at 700°C and 800°C level off. This behaviour accords with the grain structures discussed, i.e. at 1000°C, once columnar grains are established, certain orientations grow at the expense of others and  $G_R$  tends to increase with time as the oxide thickens. At 800°C, once columnar grains develop,  $G_R$  tends to be fairly steady. The temperature is sufficiently low for competitive growth of columnar grains to occur relatively slowly. At 700°C, grain growth is slow anyway, even though the grains are not columnar.

$\max. \bar{x}_C$  follows similar trends to  $G_R$  except that at 1000°C it levels off for 8 hours and 18 hours. However, these are points obtained from SEM fractographs and it is possible that  $\max. \bar{x}_C$  should continue to increase. The levelling off could be a physical effect though.

There are three possible origins for the discrepancy between  $G_R$  and  $\max. \bar{x}_C$ .

1. A geometric factor.
2. Errors.
3. A physical effect.

In equation (1) for  $k_p$ :

$$k_p = 6.4 \left\{ D^*_L + \frac{2(D_{gb}\delta)^*}{G_R} \right\}$$

the 2 is a geometric factor which arises from consideration of the grain structure in the scale as a uniform square array of grains one layer thick. This is an approximation and a change in the geometric factor, say, 1, would bring some, but not all, of the  $G_R$  and  $\max. \bar{x}_C$  points in Fig. 4 more closely into coincidence. However, it is difficult to justify such a large change in the geometric factor. The array in the

outer part of the scale, where  $\bar{x}_c$  tends to be largest, is expected to be tending to a hexagonal one (and there is evidence for this in parallel TEM). The geometric factor for a hexagonal array is  $\sim 2$ . The geometric factor is therefore unlikely to be able to account for the discrepancy.

The errors are large at 1000°C. The error bars show in Fig. 4 indicate estimates. At 700°C and 800°C, the errors are smaller and examination of the grain boundary networks for different areas suggests the max.  $\bar{x}_c$  values are a fairly good guide, despite the poor statistics. Even if the errors are strongly underestimated, it is difficult to reconcile, for instance,  $G_R \sim 1.4 \mu\text{m}$  for 4 hours at 800°C but max.  $\bar{x}_c \sim 0.4 \mu\text{m}$ . It might be argued that the areas imaged by transverse TEM are highly unrepresentative, but when 4 areas have been examined as at 21 hours for 800°C and the max.  $\bar{x}_c$  is similar for each, this argument appears weak.

It is pertinent to comment here that strictly, since an average  $k_p$  for the whole coupon is being used to deduce  $G_R$ , considering equation (1),  $(1/G_R)$  should be compared with max.  $(1/\bar{x}_c)$ . However, examination of the data showed that there was little difference between  $(1/\text{max. } \bar{x}_c)$  and max.  $(1/\bar{x}_c)$ .

The evidence therefore points to some physical effect, probably associated with the presence either of low angle grain boundaries (lagbs) or low  $\Sigma$  boundaries. Low  $\Sigma$  boundaries are boundaries where the geometric relationship between the two adjacent lattices is such that, if one were allowed to penetrate into the other, there would be a relatively high proportion of coincident lattice points.  $\Sigma$  is the inverse of the degree of coincidence. Thus, if 1 in 5 lattice points were coincident the boundary would be termed  $\Sigma 5$ .

Lagbs tend to be traced into the grain boundary networks as they are difficult to distinguish from high angle boundaries without detailed characterisation. However, lagbs are expected to have relatively low grain boundary diffusion coefficients. Hence max.  $\bar{x}_c$  would be lower than  $G_R$ . Low angle boundaries may tend to occur if texture is present. Alternatively, a proportion of the high angle boundaries might be low  $\Sigma$  boundaries. This is expected, even if the boundaries in the oxide take random misorientations with no preponderance of low  $\Sigma$ 's arising from the nature of oxide growth. There is some suggestion that low  $\Sigma$  boundaries may also be slow diffusers (e.g. 26). However, this remains to be proved

and is controversial. A considerable amount of effort would be required to check the character of grain boundaries in scales against diffusion properties and hence examine this point.

#### 4.7 Activation Energy for Grain Growth

The final question for consideration with the image analysis results centres around the activation energy for grain growth. An activation energy cannot be deduced from the results reported here, primarily because of uncertainty over which grain growth law applies whilst boundary migration is occurring. The grain size statistics would have to be improved considerably before any growth law could be chosen in preference to others. This raises difficulties with interpretation of the results of calculations of activation energies for defect migration across boundaries during boundary migration<sup>(14)</sup>. Only one value of an activation energy for grain growth in bulk NiO is reported in the literature<sup>(27)</sup>. This points to the need for further careful studies of bulk, dense NiO to ascertain, if possible, whether oxygen vacancy diffusion across the boundary does control the boundary migration process and whether impurity effects can be avoided. For scales, the statistics of the grain size data would have to be considerably improved to determine which growth law applies whilst boundaries are moving, and hence the process controlling boundary migration.

#### 5. SUMMARY, CONCLUSIONS AND SUGGESTIONS FOR FURTHER WORK

1. A (time, temperature) matrix of quantitative NiO scale grain structure information has been obtained for oxidation times between  $\frac{1}{2}$  hour and 20 hours, temperatures of 700°C, 800°C and 1000°C and at 1 atm. O<sub>2</sub>. Such a matrix had not previously been available. The 99.99% polycrystalline nickel substrates were given a light polish prior to oxidation and the oxidations were carried out under relatively high purity conditions. The grain structure information was obtained by transverse TEM, parallel TEM and SEM fractography and texture measurements were made with X-ray Diffraction. The grain boundary networks were characterised quantitatively by automatic image analysis to obtain for each grain its mean width  $x_c$  parallel to the Ni/NiO interface, its mean

length  $y_c$  perpendicular to the interface and the distance of the centre of gravity from the interface. In addition, the mean boundary radius of curvature  $k$  was found by measuring boundaries against a radius of curvature template and the number of sides  $n$  counted. Systematic Image Analysis of this kind had not previously been employed on NiO scale grain structures.

The scales were divided into layers parallel to the Ni/NiO interface and the means of the parameters found for each layer ( $\bar{x}_c$ , the columnar tendency ( $\overline{y_c/x_c}$ ),  $\bar{k}$ ,  $\bar{n}$ ).

2. The rate controlling grain size  $G_R$  was predicted from theory using measured instantaneous parabolic oxidation rates and compared with the maximum value of  $\bar{x}_c$  (max.  $\bar{x}_c$ ).  $G_R$  was always greater than max.  $\bar{x}_c$ . This discrepancy is attributed to a physical effect, possibly the fact that slow-diffusing low angle grain boundaries have been included in the traced boundary networks. A proportion of slow diffusing high angle boundaries (low  $\Sigma$  boundaries possibly) would also account for the results but this hypothesis would be difficult to prove.

3. For a given distance from the Ni/NiO interface, the average width of columnar grains is fairly constant after the first few hours, i.e. there is little lateral migration of columnar grain boundaries. This is attributed to low boundary curvature and/or low oxygen vacancy concentration in the outer parts of the scales, although impurity pinning cannot be entirely ruled out. Further experiments would be required to distinguish between these explanations.

4. Grain growth laws could not be deduced from the data for the first few hours, whilst boundary migration was occurring. Considerably more data would be required to reduce the uncertainties in examining this point.

5. Grains show increasing columnar tendency ( $\overline{y_c/x_c} > 1$ ) with increasing time and temperature. At 700°C, there is virtually no columnar tendency. These results agree qualitatively with the

suggestion that as the oxide scale thickens, the rate of nucleation of new grains at the outer surface decreases. If new grains are not formed on the surface, oxide grows on existing grains extending them lengthways so that  $y_c/x_c > 1$ . The columnar grain width is fairly constant with increasing distance from the interface at 800°C but increases slowly at 1000°C. The latter result is probably due to competition for oxide deposition between grains of different orientations, with the {220} grain orientations favoured. At 800°C, where the oxide is still thin enough for new oxide grain nucleation at the surface to be significant, the {200} grain orientation probably predominates because of favoured nucleation rather than favoured growth.

6. Adjacent to the Ni/NiO interface,  $\bar{x}_c$  increases fairly rapidly with distance from the interface. This suggests either significant grain boundary migration near the Ni/NiO interface where the grains tend to be fairly equiaxed, or larger grains because of fewer nuclei. At the interface itself, particularly at 700°C, some grain boundary pinning by grooving is probably occurring. The mean curvature per grain is high and  $\bar{n}$  low but the grain size almost constant. It is not possible to identify on the basis of this research what determines the size of grains in the region of the interface but primary recrystallisation may play a role. At 800°C, there is interaction with grain layers beyond the layer at the interface as grains at the interface appear to be shrinking whilst larger grains in the next layer grow to impinge on the interface.

7. The mean curvature per grain,  $\bar{k}$ , was found as a first step towards the "structural gradient" discussed in the literature.  $\bar{k}$  is high at the interface and decreases towards the outer part of the scale. It decreases with increasing time and temperature. The mean curvature per grain in the 2-D transverse section is a guide to the tendency for grain growth in the outer part of the scales (where it is low, little boundary migration is occurring) but at the Ni/NiO interface, particularly at 700°C, other factors intervene.

8. It is unlikely that tertiary recrystallisation is occurring. A process akin to secondary recrystallisation may take place when larger

grains in the outer part of the scale grow at the expense of smaller ones in the inner part. Primary recrystallisation may occur and this possibility merits further investigation in conjunction with developing understanding of stress generation and relief.

9. The outer surface of the NiO was highly convoluted, particularly at short times and low temperatures. At ( $\frac{1}{2}$  hour, 700°C) and ( $\frac{1}{2}$  hour, 800°C) there were regions on the Ni surface where no oxide could be detected (i.e. any oxide was  $\leq 50$  Å thick). At later times, these regions were filled in with oxide but the NiO surface was still irregular. It is notable that this island growth of NiO, which is expected at temperatures near room temperature and low PO<sub>2</sub>, persists at such high temperatures as 700°C and 800°C and at an oxygen pressure of 1 atm.. The characteristics of the island growth under the conditions of this study require further investigation in order to understand the starting conditions for microstructural evolution.

10. In addition, surface ridges are observed by SEM on 1000°C scales. These could be due to stress generation, leading to plastic deformation or Coble creep, or exaggerated oxide growth at the intersection of grain boundaries with the surface, where the nickel cation flux is relatively high. Further research is required to clarify which. At longer times at 1000°C, the surface ridges are replaced by trenches, suggesting that surface diffusion is predominating over the mechanism which is giving rise to the ridges and dispersing material over the surface.

#### ACKNOWLEDGEMENTS

I would like to thank my supervisors, Mr. A.D. Le Claire and Prof. B.C.H. Steele for their guidance, encouragement and advice; Dr. A. Atkinson, Dr. M.J. Bennett, Dr. A.T. Chadwick, Mr. D.P. Moon, Dr. P.W. Tasker and Prof. A. Rabinovitch for stimulating discussions; Mr. R.I. Taylor, Dr. J. Miaslek, Mr. G.P. Pell and Mr. D. Rickerby for helpful suggestions when I was building the high purity oxidation rig; Dr. D. Williams and Mr. F. Déslandes for help with computing; Mr. D.P. Moon, Mr. J. Desport, Miss. S. Shaw and Mr. S. Doorn, for advice and assistance with specimen preparation; Mr. J. Cook and Miss T. Halford for help in developing and carrying out the image

analysis; Mr. A.G. Morton for ICPEs of Ni coupons; Mr. A.M. Jones and Mr. B. Bellamy for carrying out XRD texture measurements; Dr. D. Rickerby and Mrs. J. Cullen for Sputter Ion Plating of transverse TEM specimens; and Dr. J. Titchmarsh and Mr. I. Vatter for assistance with STEM. The work described in this report was undertaken as part of the Underlying Research Programme of the UKAEA.

#### REFERENCES

1. Atkinson, A. Transport Processes during the Growth of Oxide Films at Elevated Temperatures. *Reviews of Modern Physics*, 57 [2] 437 (1985).
2. Atkinson, A. and Taylor, R.I. The Diffusion of  $^{63}\text{Ni}$  along Grain Boundaries in Nickel Oxide. *Phil Mag.*, A42 [4] 979 (1981).
3. Atkinson, A., Taylor, R.I. and Hugnes, A.E. A Quantitative Demonstration of the Grain Boundary Diffusion Mechanism for the Oxidation of Metals. *Phil. Mag.*, A45 [5] 823 (1982).
4. Tinker, M.T. TEM Characterisation of Microstructures Evolved during the Oxidation of Nickel. Ph.D. Thesis, Case Western Reserve University (1984).
5. Hobbs, L.W., Sawhill, H.T. and Tinker, M.T. Defect Microstructures in NiO Scales and Ni/NiO Interfaces. *Radiation Effects*, 74 291 (1983).
6. Sawhill, H.T. and Hobbs, L.W. TEM Investigation of Surface Pretreatments on the High Temperature Oxidation of High Purity Nickel. 9th International Congress on Metallic Corrosion, Toronto, 1-6 June (1984), 2' in Vol. 1.
7. Doherty, R.D. Discussion of Mechanism of Steady-State Grain Growth in Aluminium. *Met. Trans.*, 6A 588 (1975).
8. Rhines, F.N. and Craig, K.R. Mechanism of Steady-State Grain Growth in Aluminium. *Met. Trans.*, 5 413 (1974).
9. Atkinson, H.V. and Chadwick, A.T. Description and Instructions for the Oxidation Thermobalance in B552 at Harwell. AERE-M3578 (1987) in preparation.
10. Atkinson, H.V. Evolution of Grain Structure in Nickel Oxide Scales. Ph.D. Thesis, Imperial College of Science and Technology (1986).
11. Atkinson, H.V., Cook, J., Halford, T. and Rabinovitch, A. Automatic Image Analysis and Template Measurement of Grain Boundary Radius of Curvature, AERE-M3577 (1987) in preparation.
12. Mullins, W.W. The Effect of Thermal Grooving on Grain Boundary Motion. *Acta. Met.*, 6 414 (1958).

13. Rhines, F.N. and Connell, R.G. Role of Grain Growth in the Oxidation of Nickel. *J. Electrochem. Soc.*, 124 [7] 1122 (1977).
14. Atkinson, H.V. and Duffy, D.M. Calculation of Activation Energies for Defect Movement during Coincidence Grain Boundary Migration in Nickel Oxide using Computer Simulation Techniques. *Acta Met.*, 34 [12] 2371 (1986).
15. Kofstad, K.P. and Lillerud, P. On High Temperature Oxidation of Chromium. *J. Electrochem. Soc.*, 127 2397 (1980).
16. Martius, U.M. The Initial Oxidation of Nickel. *Canadian J. Physics*, 33 466 (1955).
17. Mitchell, D.F., Sawell, P.B. and Cohen, M. A Kinetic Study of the Initial Oxidation of the Ni(110) Surface by RHEED and X-ray Emission. *Surface Sci.*, 69 310 (1977).
18. Holloway, P.H. and Hudson, J.B. Kinetics of the Reaction of Oxygen with Clean Nickel Single Crystal Surfaces. *Surface Sci.*, 43 123 (1974).
19. Henrich, V.E. The Surfaces of Metal Oxides. *Reports on Progress in Physics*, 48 1481 (1985).
20. Rhines, F.N. and Wolf, J.S. The Role of Oxide Microstructure and Growth Stresses in the High-Temperature Scaling of Nickel. *Met. Trans.*, 1 1701 (1970).
21. Jiménez-Melencó, M., Domínguez-Rodríguez, A., Castaing, J. and Marquez, R. Diffusion and Creep: Application to Deformation Maps on NiO. *Scripta Met.*, 20 739 (1986).
22. Kofstad, P. On the Formation of Porosity and Microchannels in Growing Scales. *Oxid. Metals*, 24, [5/6] 265 (1985).
23. Ostyn, K.M. and Carter, C.B. On the Reduction of Nickel Oxide. *Surface Sci.*, 121 360 (1982).
24. Dubois, C., Monty, C. and Philibert, J. Influence of Oxygen Pressure on Oxygen Self-Diffusion in NiO. *Solid State Ionics*, 12 75 (1984).
25. Thompson, C.V. Secondary Grain Growth in Thin Films of Semiconductors: Theoretical Aspects. *J. Appl. Phys.*, 58 [2] 763 15 July (1985).
26. Atkinson, A. Grain Boundary Diffusion - Structural Effects and Mechanisms. *J. de Physique, Colloque C4, Supplement to No. 4*, 56, C4-379 (1985).
27. Iida, Y.J. Sintering of High-Purity Nickel Oxide. *J. Am. Ceram. Soc.*, 41 397 (1958).

Table 1  
XRD Texture Coefficients for NiO Scales

	(111)	(200)	(220)	(311)	
<u>1000°C</u>					
½ hour	0.90	0.79	1.22	1.08	(220)>(311)>(111)>(200)
1 hour	0.86	1.00	1.09	1.06	(220)>(311)>(200)>(111)
4 hours	0.76	0.65	1.28	1.32	(311)>(220)>(111)>(200)
<u>800°C</u>					
½ hour	0.63	1.50	0.84	1.03	(200)>(311)>(220)>(111)
1 hour	0.68	1.62	0.80	0.91	(200)>(311)>(200)>(111)
2 hours	0.77	1.17	1.04	1.02	(200)>(220)>(311)>(111)
4 hours	0.53	1.37	0.99	1.11	(200)>(311)>(220)>(111)
<u>700°C</u>					
½ hour	0.93	1.06	1.02	0.99	(200)>(220)>(311)>(111)
2 hours	1.32	1.78	1.01	0.90	(200)>(111)>(220)>(311)
4 hours	0.74	1.37	0.87	1.03	(200)>(311)>(220)>(111)
16 hours	0.74	1.29	1.00	0.97	(200)>(220)>(311)>(111)

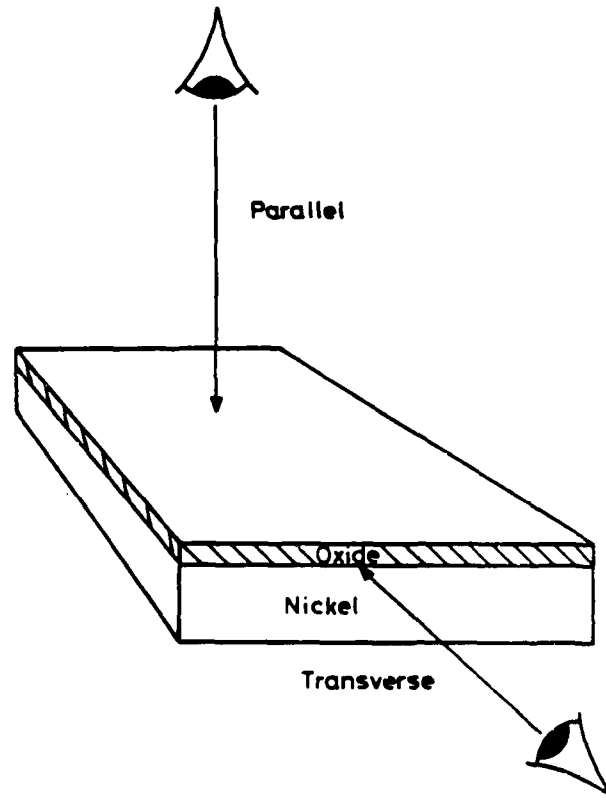


Fig.1 Diagram Illustrating Parallel and Transverse TEM Sections.

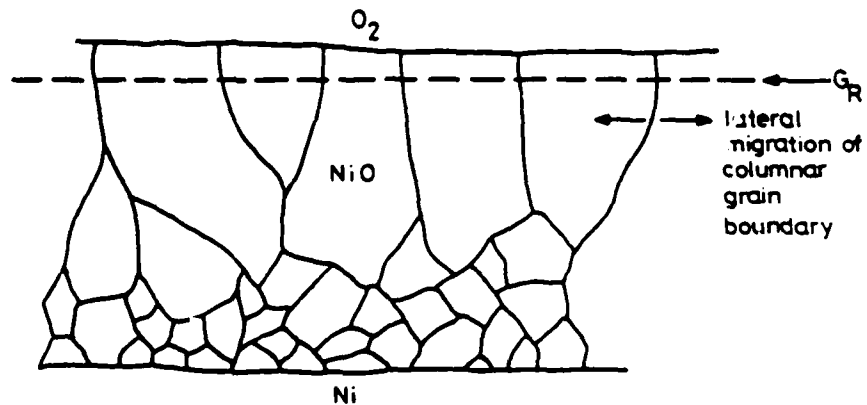


Fig. 2 Schematic Diagram Illustrating the Rate Controlling Grain Size,  $G_R$ , in a Typical  $NiO$  Scale Grain Structure.  $G_R$  is the Average Grain Width for the Outer Part of the Scale. It is the Maximum Average Width Parallel to the  $Ni/NiO$  Interface for any Plane through the Scale.

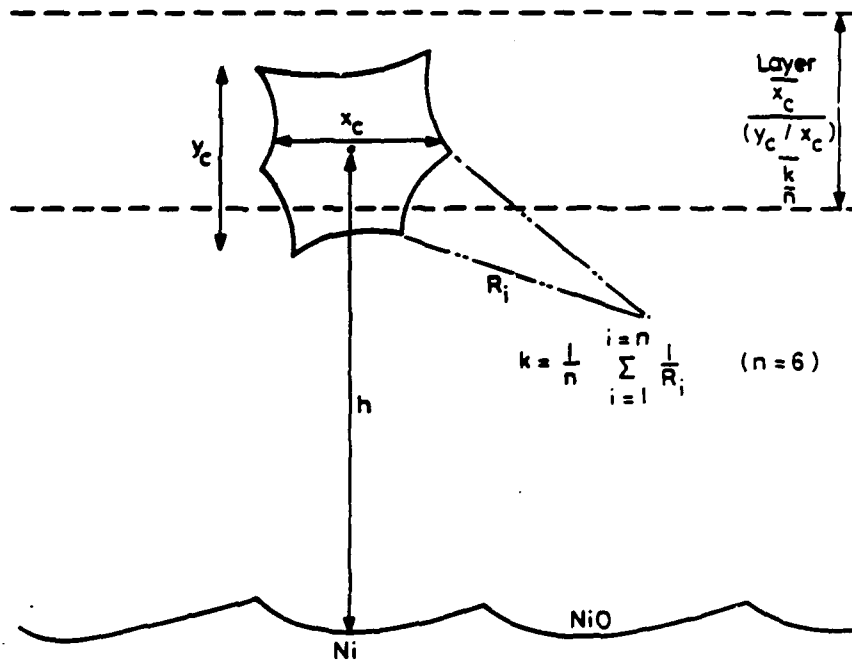


Fig. 3 Schematic Diagram Illustrating the Image Analysis Parameters.

- $x_c$  - mean chord parallel to Ni/NiO interface for the grain.
- $y_c$  - mean chord perpendicular to Ni/NiO interface for the grain.
- $h$  - distance of centre of gravity of the grain from the Ni/NiO interface.
- $k$  - mean boundary radius of curvature.
- $n$  - number of sides.

The scale is divided into layers and  $\bar{x}_c$ ,  $(\bar{y}_c / \bar{x}_c)$ ,  $\bar{k}$  and  $\bar{n}$  refer to average parameters for a given layer.

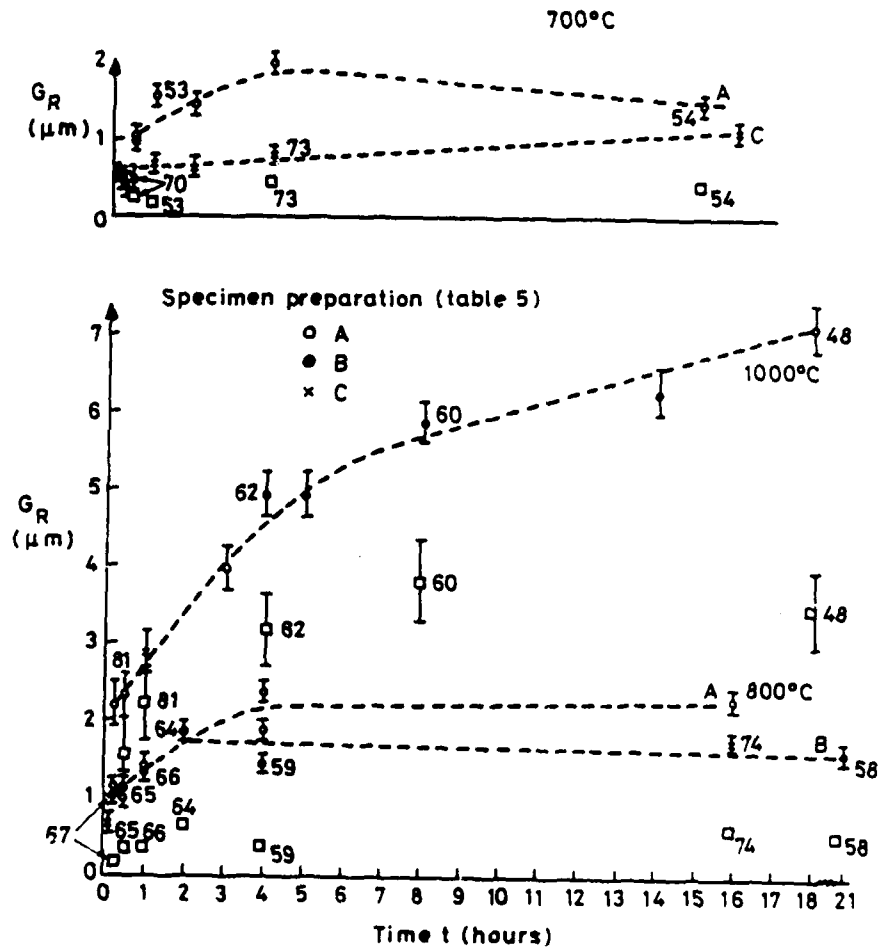


Fig. 4 . Plots of Predicted Rate Controlling Grain Size  $G_R$  Versus Time t. Lower Graph Oxidations at 800°C and 1000°C, Upper Graph Oxidations at 700°C.  $G_R$  Calculated from Weight Gain Data.  $\alpha$  Values of Max.  $\bar{x}_c$

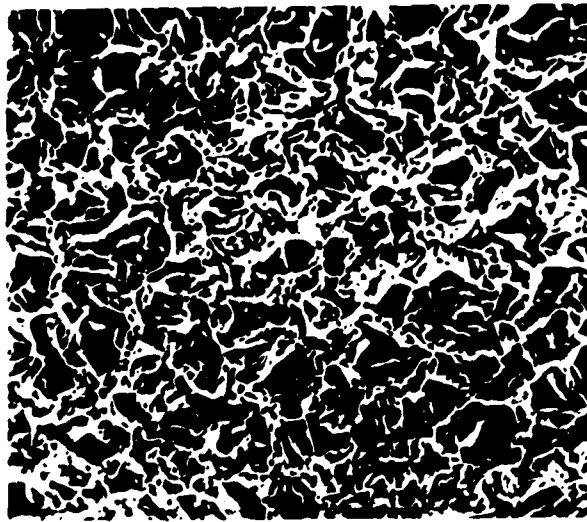


Fig. 5(a)  
Specimen 46  
1000°C  
1/2 hour

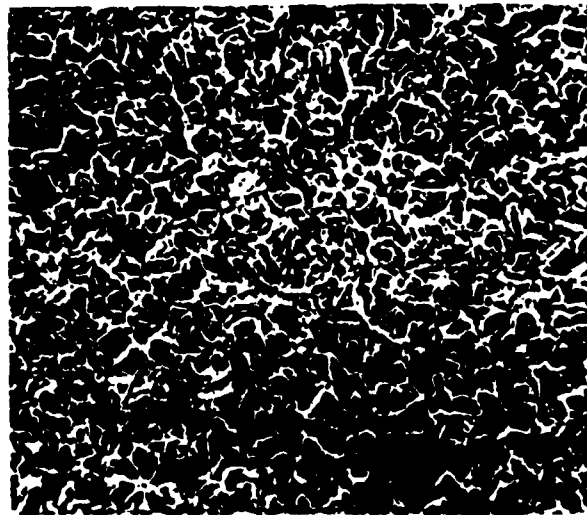


Fig. 5 (b)  
Specimen 65  
800°C  
1/2 hour

10 μm

Fig. 5 SEM Micrographs at 0° Tilt of Oxide  
Surface Morphologies after 1/2 hour Oxidation

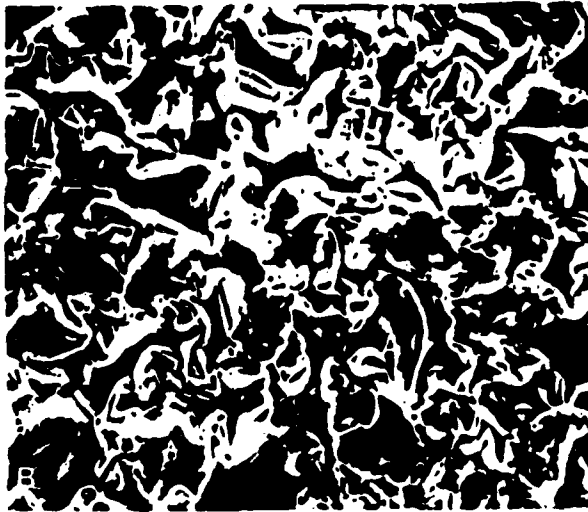


Fig. 6 (a)  
Specimen 62  
1000°C  
4 hours

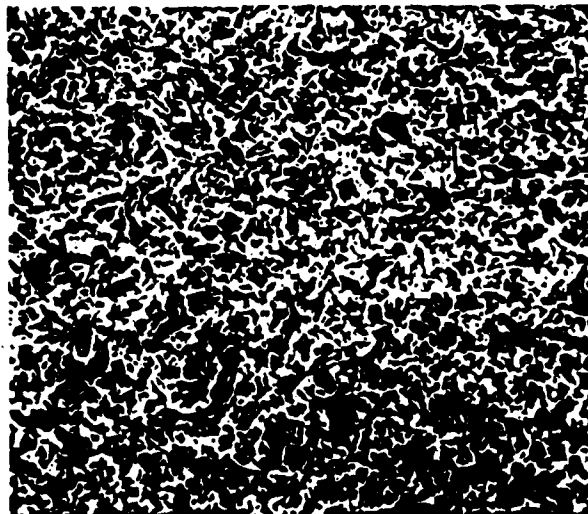


Fig. 6 (b)  
Specimen 59  
800°C  
4 hours

10μm

Fig. 6 SEM Micrographs at 0° Tilt of Oxide  
Surface Morphologies after 4 hours Oxidation



Fig. 7(a)  
Specimen 48  
1000°C  
18 hours

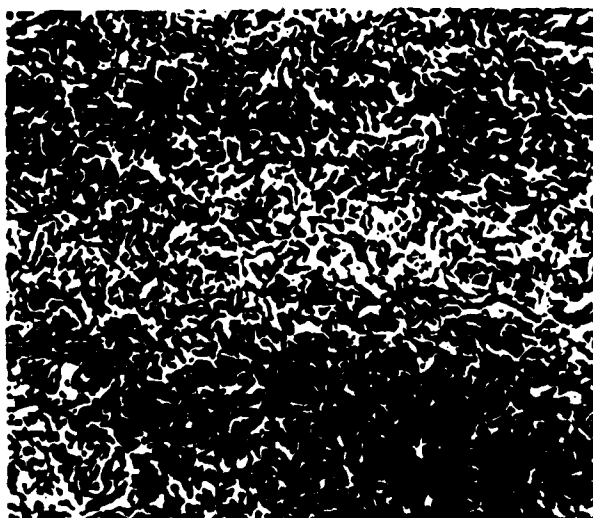


Fig. 7(b)  
Specimen 74  
800°C  
16 hours

10  $\mu$ m

Fig. 7 SEM Micrographs at 0° Tilt of Oxide  
Surface Morphologies after 16 hours Oxidation  
at 800°C and after 18 hours at 1000°C



Fig. 8 (a) Scale Grown at  
1000°C for 1/2 hour  
(Specimen 46)

—  
1μm

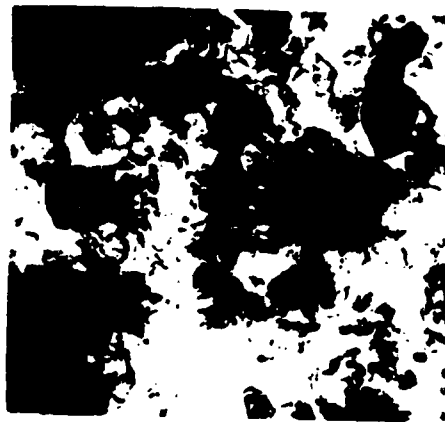


Fig. 8 (b) Scale Grown at  
800°C for 1/2 hour  
(Specimen 65)

—  
1μm

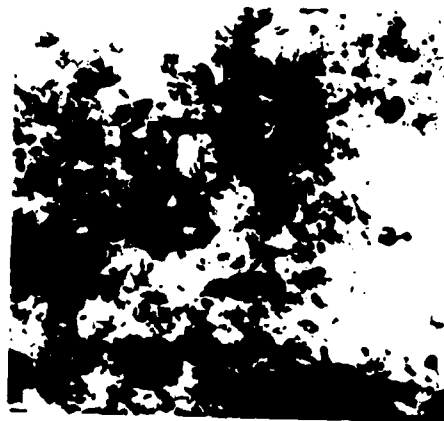


Fig. 8 (c) Scale Grown at  
700°C for 1 hour  
(Specimen 53)

—  
1μm

Fig. 8. Parallel TEM Micrographs of Stripped  
Nickel Oxide Scales



1  $\mu$ m

Fig. 9. Parallel TEM of Stripped Nickel Oxide Scale Grown at 800°C for 4 hours (Specimen 59)

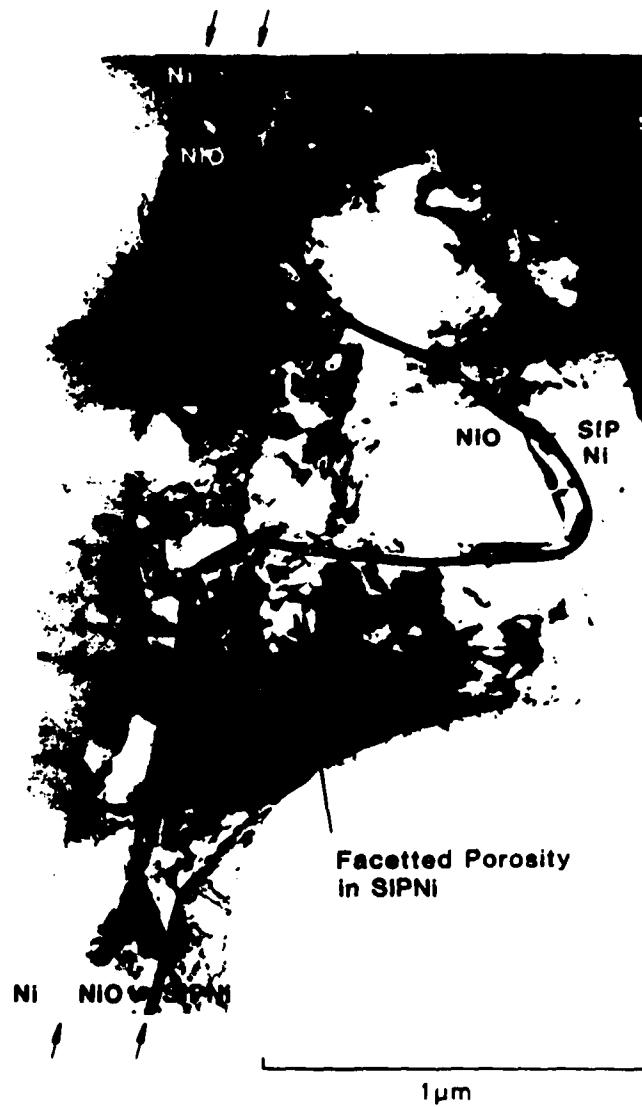


Fig.10. Transverse TEM Micrograph of Scale  
Grown on Ni at 700°C for 2 hours (Specimen 72)  
Showing Convolution of the Outer Surface of the Oxide



Fig. 11. Transverse TEM Micrograph of Scale Grown on Ni at 800°C for 21 hours (Specimen 58)

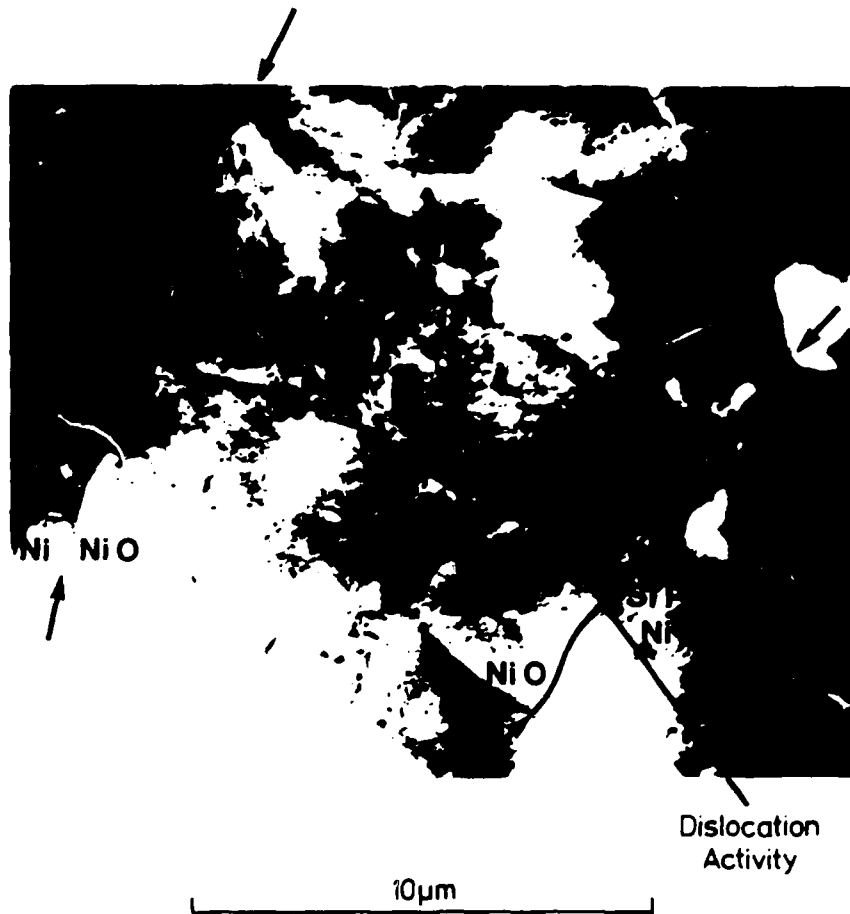


Fig.12. Transverse TEM Micrograph of Scale Grown on Ni at 1000°C for 4 Hours (Specimen 62)

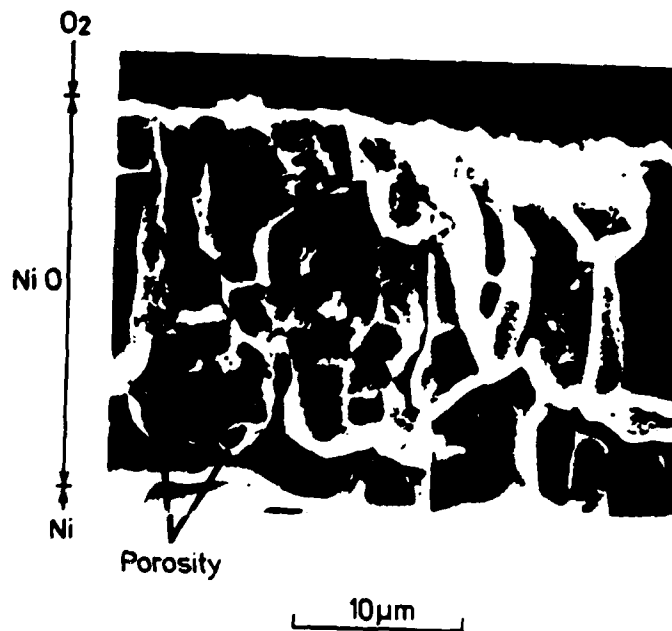


Fig.13. SEM Micrograph of Transverse Fracture Section through Scale Formed on Nickel at 1000°C for 18 Hours in 1 atm.  $O_2$  (Coupon 48)

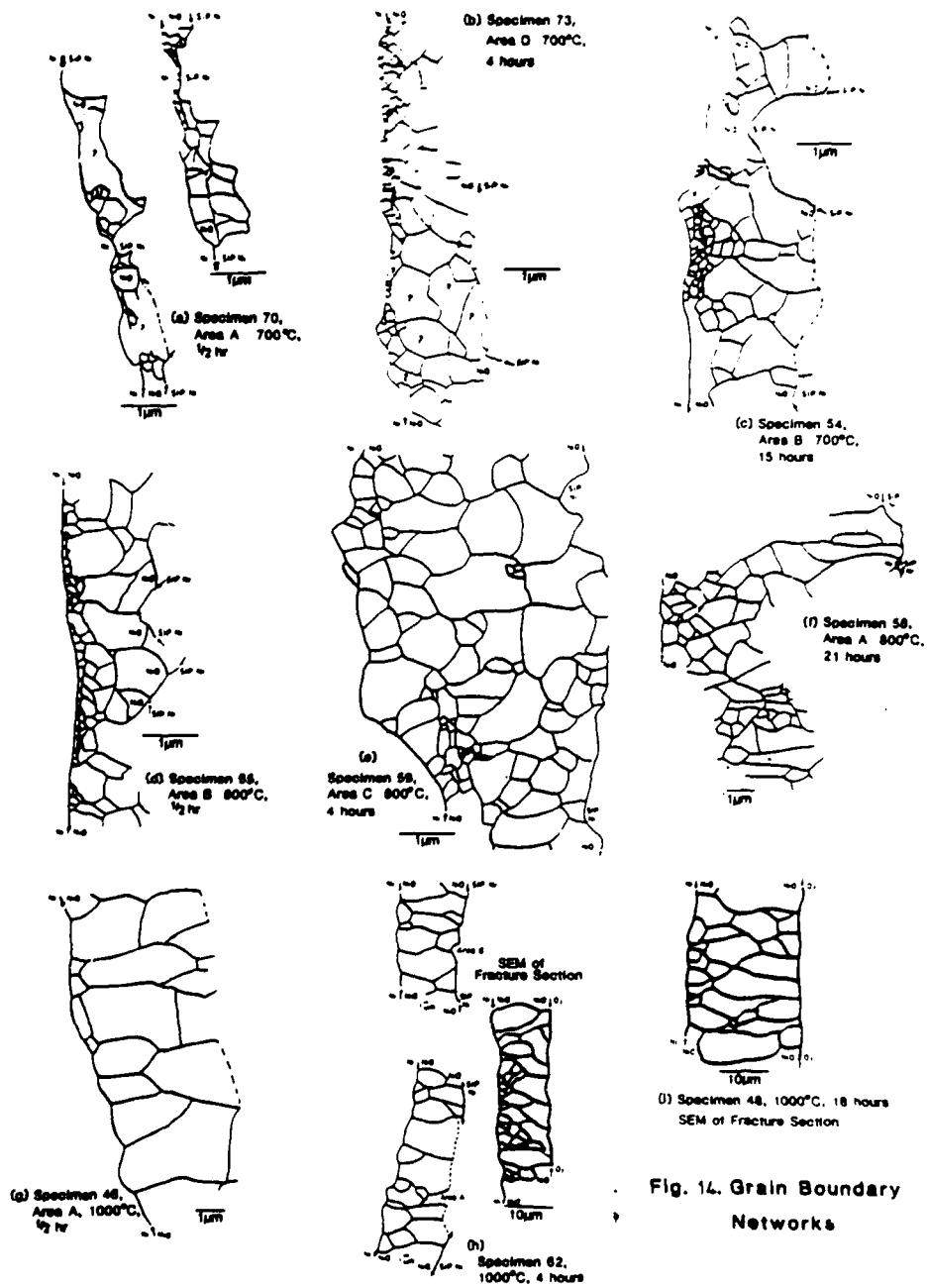


Fig. 14. Grain Boundary Networks

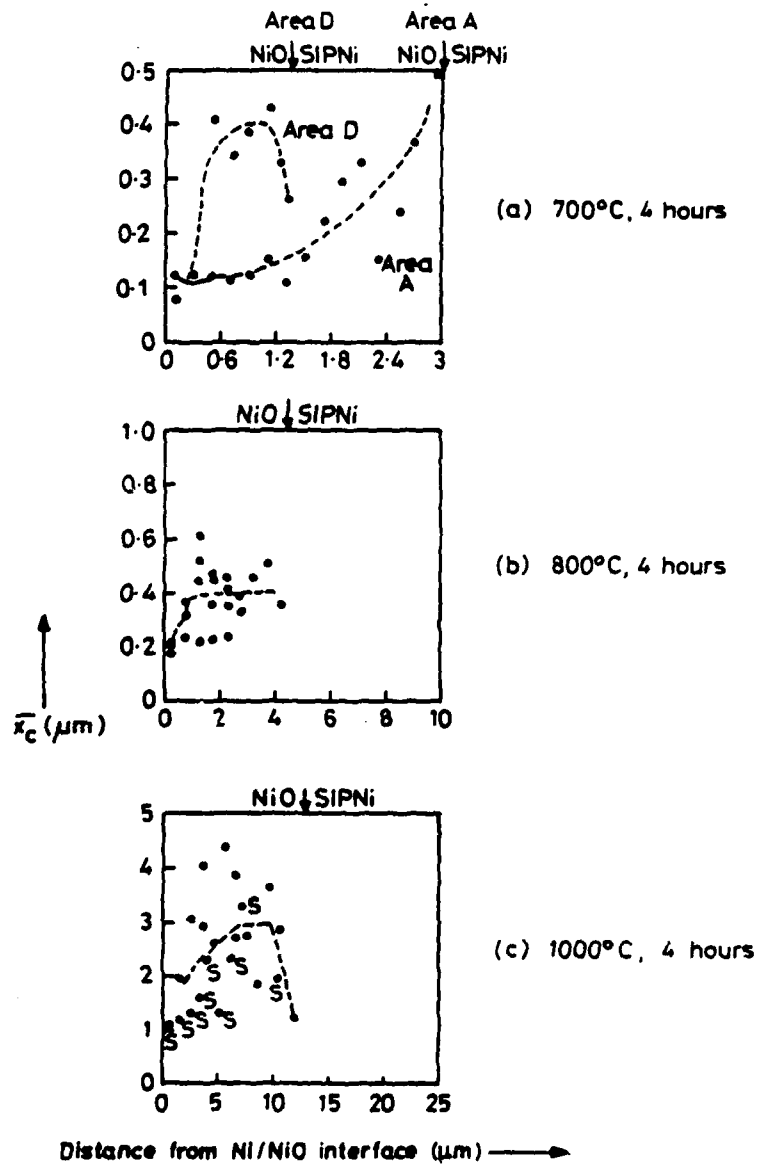


Fig. 15 Plots of  $\bar{x}_c$  Versus Distance from the Ni/NiO Interface. Points Marked with S from SEM rather than TEM.

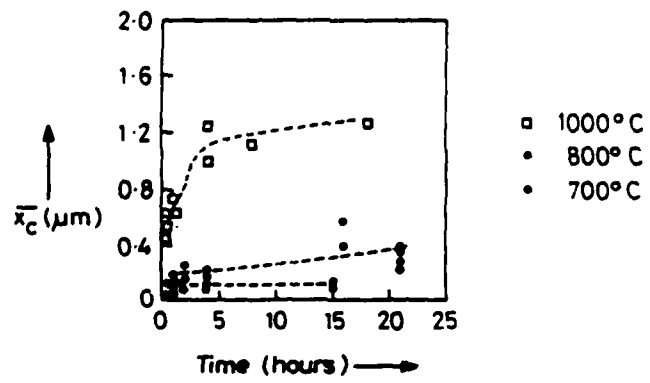


Fig. 16 Plot of  $\bar{x}_c$  Versus Time for Layer Adjacent to the Ni/NiO Interface.

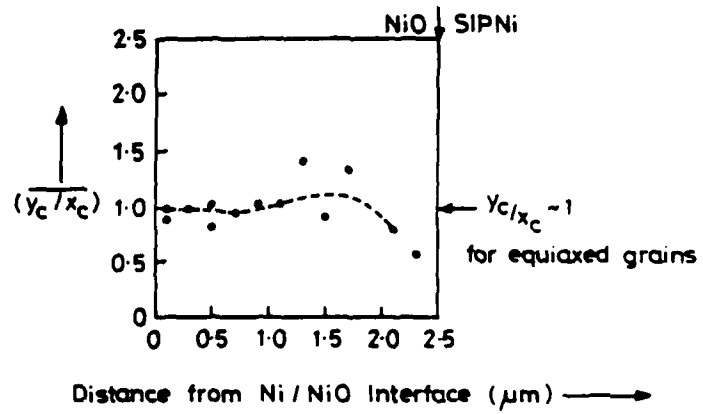


Fig. 17 Plot of  $(\overline{y_c / x_c})$  Versus Distance from the Ni / NiO Interface for Scale Grown at 700°C for 15 hours.

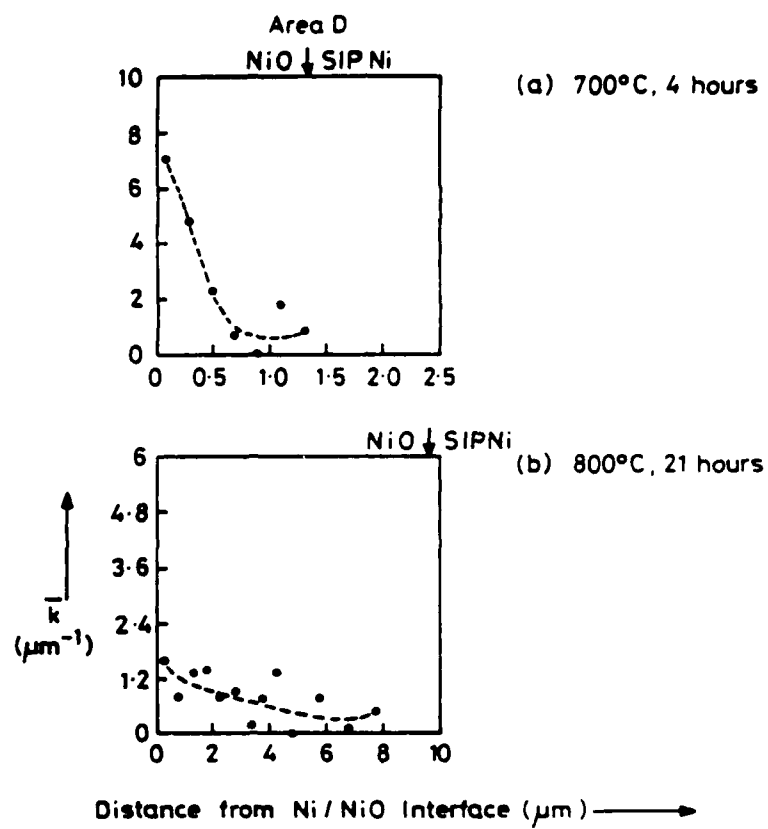
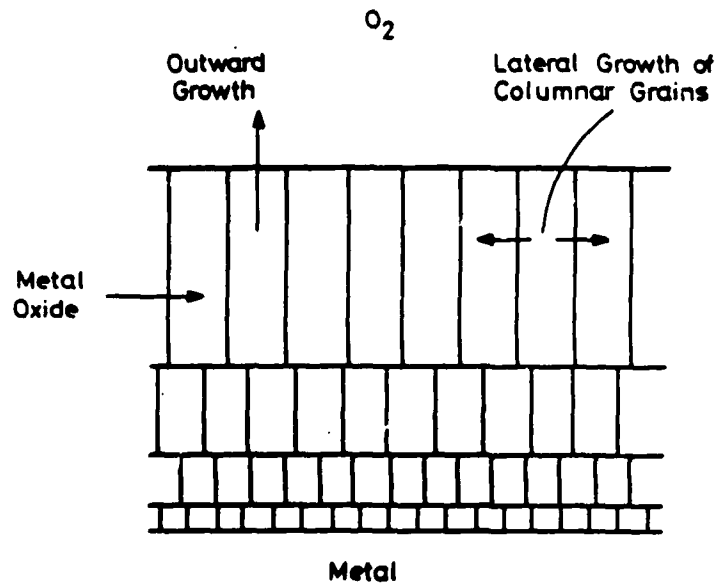


Fig. 18 Plots of Mean Curvature / Grain,  $\bar{k}$ , versus Distance from the Ni/NiO Interface



**Fig. 19** Scale Microstructure Resulting from Decrease in Nucleation of New Grains at Outer Surface as Oxide Thickens According to Tinker (1984)  
Outer Columnar Grains can Grow Laterally

END  
FILMED MARCH 1987

END

DATE

~~FILMED~~

4 88

ITL